Turkish Journal of Engineering
https://dergipark.org.tr/en/pub/tuje
e-ISSN 2587-1366

# Collapse capacity assessment of non-ductile open ground story reinforced concrete frame

**Emre Akın** [*1], **Emad Kanas** [1]

[1]*Mersin University, Civil Engineering Department, Türkiye*
[2]*Adnan Menderes University, Civil Engineering Department, Türkiye*

**Keywords**
Reinforced Concrete
Infill Wall
Soft Story
Open Ground Story
Collapse Capacity

**Research Article**
DOI: 10.31127/tuje.1071965

Received: 11.02.2022
Accepted: 25.04.2022
Published: 26.04.2022

**Abstract**

It is a well-known fact that the absence of infill walls at the ground story, which is termed as "open ground story" may lead to a soft-story deficiency, especially in the case of non-ductile buildings. The previous severe earthquakes have shown that catastrophic destruction may occur in such a condition. Therefore, the seismic assessment of open ground story reinforced frames, where the effects of infill walls are incorporated, is of vital importance. However, the effects of infill walls are generally disregarded or considered indirectly in the seismic assessment procedures of the codes. This may mislead the actual condition of the open ground story buildings at different performance levels. This study aims to assess a non-ductile reinforced concrete frame with an open ground story regarding the collapse prevention performance level. The pushover and incremental dynamic analyses results are evaluated following the code limitations for collapse prevention. The results demonstrate the measure of misleading caused by the ignorance of infills at the upper stories while applying these code limitations.

## 1. Introduction

The previous studies reveal the influence of infill walls on the lateral behavior of buildings by a consideration of numerous parameters [1-7]. Yet, the knowledge of these members has been improving with the aid of latest analytical tools and models. The non-uniform placement of infills along the building elevation or in plan causes stiffness and strength irregularities [8-9]. The most common example is the open ground story (OGS) in which case the infills are absent in one story (generally the ground story). The OGS has the potential to cause soft/weak story deficiency which may depend on the characteristics of the structural system, masonry infills and ground motion [10]. Although there are certain regulations entailed by the codes to prevent soft/weak story deficiency [11-12] in the design, the assessment of existing buildings with OGS that were constructed in the absence of these regulations is a critical issue. A more approximate seismic assessment of these types of buildings requires taking the effects of infill walls into account.

In the current study, the collapse performance of a reinforced concrete frame that does not comply with the current seismic design principles is assessed by comparison with the collapse prevention limits suggested by various seismic codes. The nonlinear pushover and incremental dynamic analyses were conducted for this purpose. The frame models were considered to have either OGS or not. To be used in the time history analyses, eleven selected earthquake ground motion records were matched with the design spectrum.

## 2. Numerical modeling

Seismostruct software [13] was used for the nonlinear analyses of the five-story, two-span planar RC frame. The frame that is illustrated in Fig. 1 belongs to an existing building which was also used by Kadaş [14]. However, some slight alterations were done in the dimensions and reinforcement details of the members as given in Table 1, to obtain non-ductile structural characteristics. No additional cross ties were used for the confinement of the sections (i.e., only hoop reinforcement with two legs along both sectional directions). The characteristic compressive strength of

* **Corresponding Author**

*(eakin@mersin.edu.tr) ORCID ID 0000-0003-1936-8916
(imad_alkanas@hotmail.com) ORCID ID 0000-0002-5905-4172

**Cite this article**

Akin, E., & Kanas, E. (2023). Collapse capacity assessment of non-ductile open ground story reinforced concrete frame. Turkish Journal of Engineering, 7(2), 157-165

concrete was 15 MPa. The characteristic yield strength of all reinforcements was 220 MPa.

The lateral response of the floor levels was assumed as a rigid diaphragm. The uniformly distributed beam dead loads were 12.36 kN/m in the first four stories and 9.62 kN in the last story. The live loads were 0.98 kN/m on all beams, except those at the roof where it had a value of 0.49 kN/m. The concrete specific weight was considered as 24 kN/m$^3$. The specific weight was 8 kN/m$^3$ for the infills. The second-order effects are considered in all analyses.

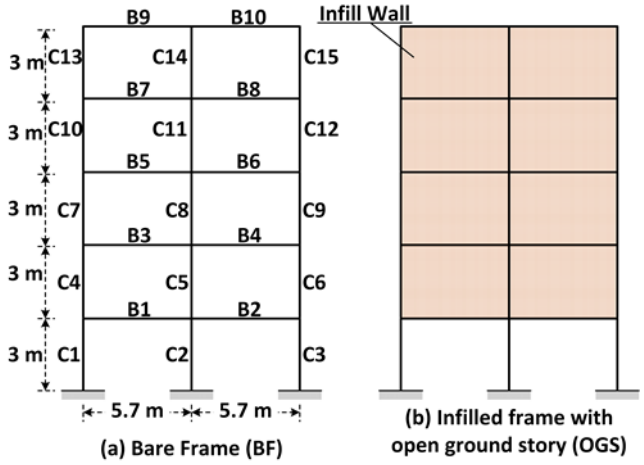


**Figure 1.** The models of (a) bare and (b) OGS frames

**Table 1.** The properties of the beams and columns

| Section | Dimensions (mm×mm) | Longitudinal Reinforcement | Transverse Reinforcement |
|---|---|---|---|
| Column | 500×500 | 10ϕ18 | ϕ8/200 mm |
| Beam-Support | 250×600 | 6ϕ18 (top)<br>4ϕ18 (bottom) | ϕ8/200 mm |
| Beam-Span | | 4ϕ18 (top)<br>6ϕ18 (bottom) | ϕ8/200 mm |

The nonlinear model which is compatible with the relationship proposed by Mander et al. [15] and the cyclic rules of Martinez-Rueda and Elnashai [16] was employed for the concrete. The elastic modulus was calculated as 18200 MPa for the concrete according to ACI [17]. The strain at the ultimate strength of concrete was considered as 0.002 in compression. The modulus of elasticity was 2×10$^5$ MPa for the steel reinforcement. The strain hardening was considered with a ratio of 0.005 for the steel. A distributed inelasticity model which was the inelastic force-based frame element of Seismostruct was employed for the RC members. Four integration sections were used, where a meshing with 100 fibers was conducted. The initial and final beam integration sections were formed by using the support sectional properties (Table 1) and the properties for the span sections were assigned to the others.

The masonry wall properties that are defined as "fair" quality by the American Society of Civil Engineers (ASCE) [18] were employed for the infill wall model of this study. Accordingly, the compressive strength ($f_m'$), modulus of elasticity ($E_m$) and shear strength of the infill walls were quantified as 4.1 MPa, 2255 MPa and 0.14 MPa, respectively. The four-node inelastic infill panel element of Seismostruct software which consists of two struts for the axial response and one strut for the shear response along each diagonal direction was employed for the nonlinear modeling of infill walls. The same definitions and assumptions are followed to constitute the infill wall models as described in a previous study by the first author Akın [10]. Therefore, these will not be repeated here once again to keep it abbreviated.

## 3. Analyses

### 3.1. Pushover Analyses

The eigenvalue analyses resulted in a fundamental vibration period of 1.13 s. for the BF and 0.71 s. for the OGS. Besides, the mode shape vector, {Φ} and mass matrix, [m] were taken for the first (fundamental) modes. The generalized mass ($M_1$), base shear effective modal mass ($M_1$*) and other modal properties ($L_1$ and $\Gamma_1$) were estimated in the first mode (designated by the subscript "1") by using Eqns. (1)-(4). In these expressions, $m_j$ is the total mass in the "j"th story and $\Phi_{j1}$ is the modal lateral deflection at the "j"th story corresponding to the first mode.

$$M_1 = \sum_{j=1}^{N=5} m_j \times \phi_{j1}^2 \quad (1)$$

$$L_1 = \sum_{j=1}^{N=5} m_j \times \phi_{j1} \quad (2)$$

$$\Gamma_1 = L_1/M_1 \quad (3)$$

$$M_1^* = \Gamma_1 \times \mathrm{M}_1 \quad (4)$$

The static pushover analyses (SPO) were conducted under lateral loading where the pattern of nominal loads was assumed as inverse triangular. These nominal lateral loads at the stories were allocated to each node according to the nodal masses. Fig. 2 illustrates the design spectrum that was utilized to determine the displacement at the target point. The design spectrum was determined for the location of the original building in accordance with the previous version of the Turkish Earthquake Code (TEC [19]) that was the official code at the time when this study started. An earthquake level corresponding to 475 years of return period was chosen for the design spectrum. The damping ratio was considered as 5%. The region of the design spectrum with constant acceleration was bounded by the corner periods of 0.10 s. ($T_A$) and 0.48 s ($T_B$). The capacity curves obtained by SPO analyses were converted into the spectral coordinates of the design spectrum. This was accomplished by converting base shear, $V_b$ into spectral acceleration, $S_a$ and roof drift, $\delta_{roof}$ into spectral displacement, $S_d$ by utilizing Eqns. (5) and (6), respectively. $\Phi_{N1}$ is the modal lateral deflection at the roof level for the first mode (i.e., j=N).

$$S_a = V_b/M_1^* \quad (5)$$

$$S_d = \delta_{roof}/(\phi_{N1} \times \Gamma_1) \quad (6)$$

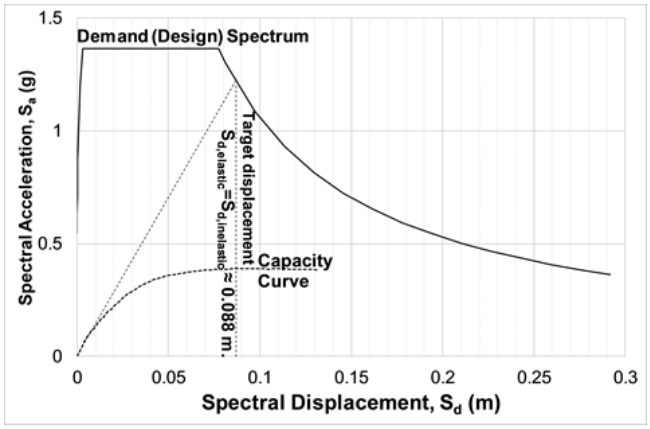


**Figure 2.** Estimation of the target displacement in the BF

The fundamental vibration periods ($T_1$) of all models were larger than $T_B$ (upper limit for the region of constant acceleration). This enabled the utilization of the rule which states that the inelastic displacement demands, $S_{d,inelastic}$ may be taken as equal to the elastic displacement demands, $S_{d,elastic}$. Fig. 2 illustrates the determination of the displacement at the target point according to the TEC [12] for the bare frame. These spectral displacements could be converted to roof displacements at the target point by an inverted utilization of Eq. (6). This yielded a roof displacement of 0.113 m for the BF and 0.078 m for the OGS. The SPO analyses were conducted again up to a step where these determined roof displacements were attained. And finally, the inelastic demand parameters were obtained for the columns.

### 3.2. Incremental Dynamic Analyses (IDA)

The incremental dynamic analyses of the models were conducted under gradually increasing intensity of the applied acceleration time history records by use of scaling factors, changing between 0.1 and 1.3 with an increment of 0.2 at each step. During the analyses of some models, the convergence problems occurred and the analyses should have to be terminated before attaining the scale factor of 1.3. Even so, the quantity of the analysis steps was enough for a reasonable evaluation of the results in all cases. Eleven ground acceleration records, each belonging to a different event, were chosen for the IDA. The records were taken from the Pacific Earthquake Engineering Research Center (PEER) "NGA-West 2" database in conformity with a seismic scenario chosen according to the location of the building [19]. The parameters that were taken into account for this seismic scenario are listed in Table 2.

The chosen ground motion records were Darfield-New Zealand-2010, Duzce-Turkey-1999, Erzincan-1992, Imperial Valley-02-1940, Landers-1992, Kobe-Japan-1995, Kocaeli-Turkey-1999, Parkfield-1966, Sierra-Mexico-2010, Superstition Hills-02-1987, Tottori-Japan-2000. SeismoMatch software [20] was utilized to match the response spectra of these ground motion records with the design spectrum. The matching was completed in two steps having a maximum of 30% misfit tolerance. The matching was continued up to the periods of 1 s. and 4 s in the first and second steps, respectively. The spectra that were matched with the design spectrum are shown in Fig. 3. The period of each model at the first mode and upper boundary for the constant acceleration zone, $T_B$ is also marked in Fig. 3. These matched ground acceleration records were used for the IDA.

**Table 2.** Specifications of the seismic scenario

| Parameter | Interval/Property |
|---|---|
| Type of Fault | Strike-Slip |
| Magnitude of Earthquake | 6.0-7.8 |
| Distance of Rupture ($R_{RUP}$) (km) | 0-100 |
| Distance of Joyner-Boore ($R_{JB}$) (km) | 0-30 |
| Shear Wave Velocity at the top 30 m of the subsurface (Vs30) (m/sec.) | 100-400 |

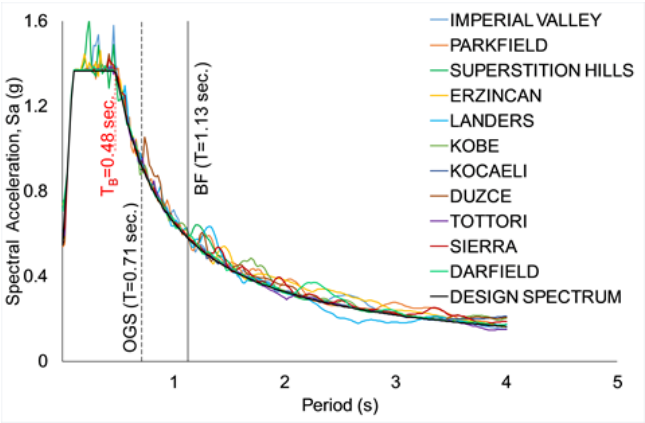


**Figure 3.** The spectrums of the chosen ground acceleration records matched with the design spectrum

## 4. Discussion of results

### 4.1. Results of SPO Analyses

The pushover curves are presented in Fig. 4 where the estimated target lateral drift at the roof level is also presented for the models. The non-ductile characteristic of both frames is explicit in this figure with a negative slope during the plastic phase of the response. When the capacity curves of both models are compared, the considerable increase in the initial rigidity of the OGS model compared to BF is clear. This is notable since it is attributed to the addition of infills in the absence of those at the ground story. A consequent alteration of the base shear demand may be expected in the OGS model due to the increased rigidity. On the other hand, it is obvious in Fig. 4 that there is no considerable base shear capacity increase in the OGS model in comparison to BF that may countervail the altered demands.

At this stage, a probable concentration of inelastic demand parameters in the ground story columns of the OGS model compared to BF is evaluated. The concrete strain values at the columns of only the ground story are considered in this evaluation. However, the base shear demands and chord rotations at the ground and first story levels are taken into account for comparison. In Fig. 5, these demand parameters are assessed with respect to the limiting values of Eurocode 8 [11] and TEC [12] at different damage states. Here "SD" and "NC" correspond to the "Significant Damage" and "Near-Collapse" limit states of Eurocode 8, respectively. These limit states are

designated as "Controlled Damage" and "Collapse Prevention" in the TEC [12], respectively.

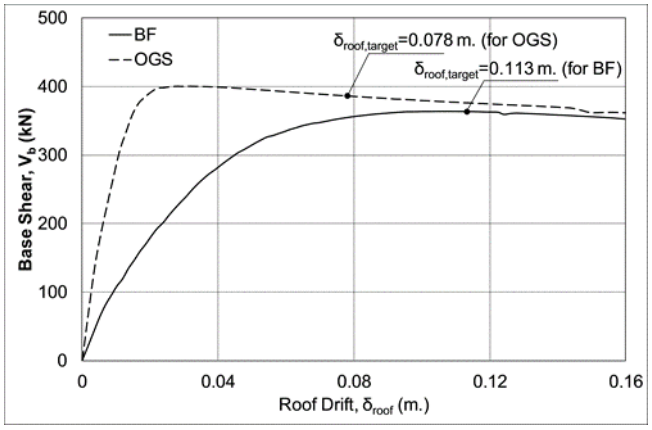


**Figure 4.** The static pushover analyses results of the BF and OGS models

The column sectional details that are provided in Table 1 and the properties of the materials given in the preceding sections were used for the calculation of the limit values of the codes. The resulting chord rotation capacity values are 0.0096 rad and 0.0128 rad at the SD and NC limit states, respectively. The NC limit in terms of shear force capacity was estimated as 163.8 kN. These limit values for the chord rotation and shear force were calculated according to the Eurocode 8 (i.e., sections A.3.2 and A.3.3 of part 3). On the other hand, section 5.8.1.1 of the TEC [12] was utilized to estimate the concrete strain capacity values of 0.0051 and 0.0068 for the SD and NC limit states, respectively. In Eurocode 8, the parameter that is employed to distinguish the priority of the members in terms of seismic resistance of the structure ($\gamma_{el}$) was taken to be 1.5 for the columns (as a primary element). The ratio between moment and shear at the end section was considered to be one-half of the column height as recommended by the TEC [12]. In the calculations of the limit states, the axial load on the columns was assumed as 560 kN. This value is the mean value for the highest axial loads at the ground story columns which occurred during the IDA step corresponding to the NC stated by FEMA 350 [21]. The definition of the NC limit using the IDA results according to FEMA 350 will be given in the next section. Only the reinforcements at the ends of the section (4ϕ18) were regarded as the tension or compression reinforcements. In other words, the probable contribution of the reinforcement at the mid-section (2ϕ18) to the tensile or compressive response was ignored. No diagonal reinforcement was considered since there is none in the section (i.e., $\rho_d$=0). The confinement effectiveness factor (α) was estimated as 0.42 with the same definition in Eurocode 8 [11] and TEC [12]. During the calculations according to Eurocode 8, the capacities were reduced with regard to the insufficient seismic detailing and the use of smooth bars for the longitudinal reinforcements. While applying these reductions, the longitudinal reinforcements were regarded as lapped at the member ends, which is a typical application for most of the buildings in Turkey. The length of the lapped bars ($l_o$) was assumed as equal to 50 times the diameter of the bar ($d_{bL}$). In the concrete strain capacity calculations according to TEC [12], only 30 percent of the lateral reinforcement was taken into account due to the use 90° hook ends of the stirrups as suggested by the code.

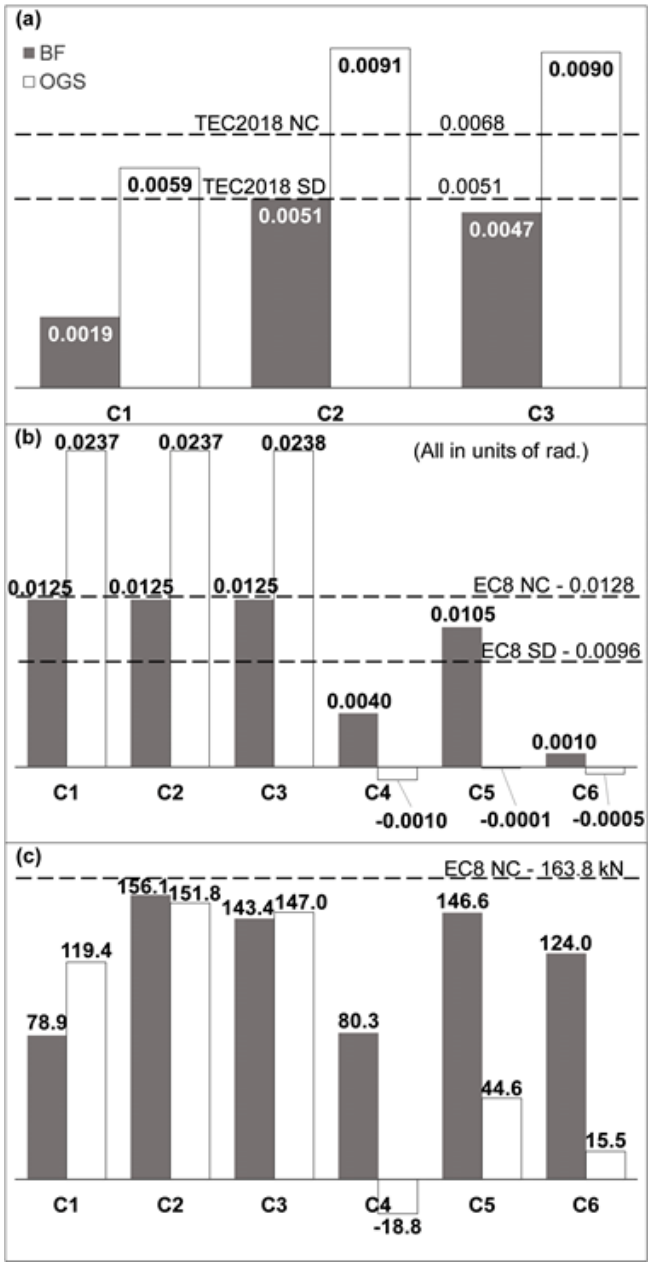


**Figure 5.** The results of the SPO analyses: (a) maximum concrete strain on the columns of the ground story, (b) maximum chord rotations and, (c) maximum shear forces on the columns of the ground and first stories

According to the TEC (2018) classification in terms of the concrete strain, one column (C2) exceeds the SD limit, and one other column (C3) is approximate to this limit at the ground story (Fig 5(a)). The concrete strain of the columns in the OGS model is larger compared to BF even though these values were obtained at a smaller target displacement in the OGS frame (Figs 4 and 5). Two columns (C2 and C3) go beyond the NC limit and one column (C1) exceeds the SD state at the ground story of the OGS model. All columns at the ground level and one column at the upper story of the BF remain in between the SD and NC limits when the Eurocode 8 definition in terms of chord rotation is considered (Fig. 5(b)). In the

OGS frame, the chord rotations of columns at the ground story increase substantially and go beyond the NC limit state. On the other hand, there was an abrupt decrease in the chord rotations of the first story columns in this frame compared to BF. In this story, the observed negative chord rotations may be attributed to the contribution of higher modes of vibration due to the irregular distribution of rigidity in the OGS model. It should be noted that the assessment of Eurocode 8 according to the chord rotation may be regarded as more conservative in comparison to that of TEC [12] with respect to the local strain obtained by SPO analyses. This was especially notable for the BF model. There was no major difference between the OGS and BF concerning the column shear demands at the ground story (Fig. 5(c)). As one may anticipate, there was a considerable decline in the shear demands of the first story columns owing to the infills of the OGS frame compared to BF.

### 4.2. Results of IDA

To be comparable with the SPO results, in the IDA analysis, the base shear was determined as the “intensity measure" and roof drift was chosen as the "engineering demand parameter”. The consequent IDA curves of all ground acceleration records are given in Fig. 6(a). The statistical 16%, 50% (median) and 84% fractile curves are presented in Fig. 6(b). When the IDA results of bare and OGS frames are statistically compared, it may be stated that the dispersion is higher for the OGS in comparison to BF.

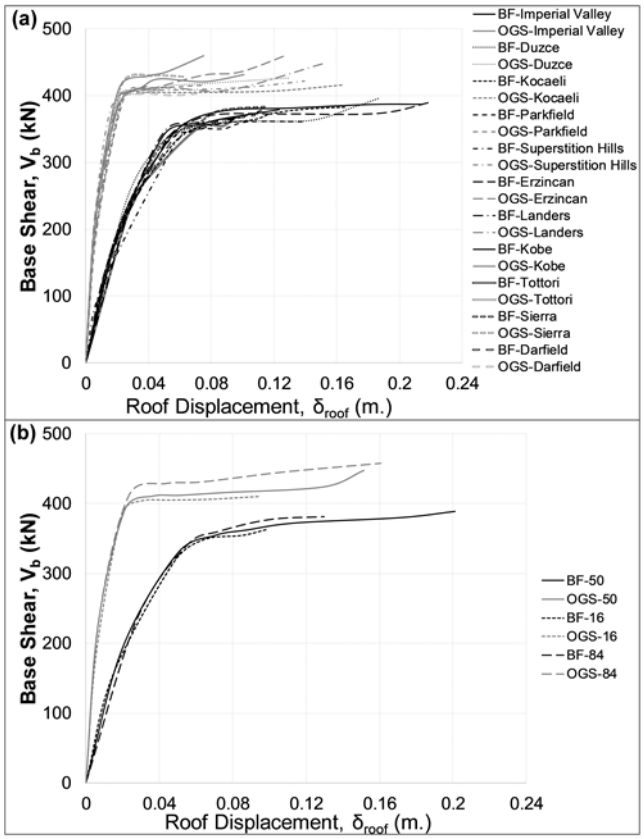


**Figure 6.** The incremental dynamic analysis curves of BF and OGS frame: (a) under all acceleration records, (b) 16%, 50% (median) and 84% fractile curves

Referring to FEMA 350, Vamvatsikos and Cornell [22] assume that the near-collapse limit is defined either by the point where the local slope of the IDA curve attains 20% of the initial (i.e., elastic) slope or maximum inter-story drift ratio extends to 10% for the steel moment-resisting frames. In this study, the definition that states an 80% reduction in the initial rigidity is considered to determine the NC limit state by a graphical rendition of the IDA curves. The same definition of Eurocode 8 for the NC limit state in terms of chord rotation (i.e., 0.0128 rad) that was used in the previous section is also evaluated here. Additionally, the concrete strain limit value of the TEC [12] for the NC (i.e., 0.0068) which is generally more critical compared to the strain of reinforcement is also considered in this part once again. It is worth noting that none of these limit state definitions, except the graphical rendition proposed by Vamvatsikos and Cornell [12] take the infills into account during the assessment of the building. A graphical definition for the limit states naturally considers all structural characteristics, such as the effect of infill walls assigned to the model.

The point corresponding to an 80% reduction in the initial rigidity (i.e. NC limit state of FEMA 350) is shown in Fig. 7 on the median IDA curves as exemplarily. This procedure was applied for the IDA curves of all models under each ground acceleration record where the IDA step nearest to this level was designated as the limit for the NC. Eventually, the local values for the chord rotation and concrete strain are obtained at this limit. The median, 16th and 84th percentile of these demands obtained from the representative column “C2” are presented in Fig. 8 together with the code limits for the NC state.

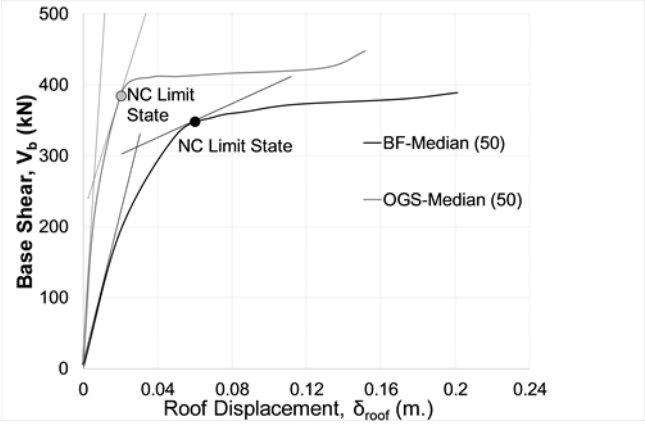


**Figure 7.** The graphical definition of the near-collapse (NC) limit state according to FEMA 350

As shown in Fig. 7, the limit for the NC is determined at the transition part of all curves between the initial (ascending) portion and the flat (or almost flat) remaining portion. The NC was experienced at a smaller roof drift in the case OGS frame in comparison to BF. There may be two reasons for this: the initial rigidity of the OGS model is higher and the transition from the initial region to the remaining flat region is sharper in the case of OGS in comparison to BF. This caused a reduction in the demand values of the OGS frame at the NC limit state

as exemplarily shown in Fig. 8 for column C2. It should be noted that this result was also the case in the other columns of the ground story.

When compared with the graphical method of FEMA-350 [21], the TEC [12] seems to be slightly more conservative while describing the NC limit state for the BF by employing the strain in the columns (Fig. 8(a)). However, this was not the case in the OGS frame and the limit for the NC is experienced earlier with regard to FEMA 350. The NC limit defined by Eurocode 8 according to the chord rotation was much larger than the one determined by FEMA 350 for the ground story columns of both types of frames (Fig. 8(c and d)).

The plastic hinge formations throughout the structure were designated to evaluate the description of FEMA 350 for the near-collapse limit. The plastic hinge formation was identified by observing the hysteretic moment-rotation diagrams at the integration sections of the members. This was done at the IDA step which was specified as the limit for the NC. The consequent moment-rotation diagrams at the initial sections of columns C1 and C4 are presented in Fig. 9. An "idealized yield point" has been transcended by the initial section of column C1, so that the plastic hinge formation can be defined (Fig. 9(a)). However, the bottom section of column C4 has not experienced any inelastic response (Fig. 9(b)).

The resulting distributions of the plastic hinges in the IDA step specified as NC limit by FEMA 350 and the following step are illustrated in Fig. 10 for the Duzce record. The maximum column chord rotations formed at the ground story corresponding to these steps are also denoted in the same figure. According to Fig. 10(a), the number of plastic hinges was not adequate to result in collapse (i.e., unstability) when the NC limit defined by FEMA 350 was reached for the BF (i.e., chord rotation equals 0.0074). On the other hand, the collapse was formed at the first two-story levels in the following step when the ultimate chord rotation of the ground story columns attained 0.0113. It may be stated that the collapse seems to form immediately after the FEMA 350 NC limit. Consequently, the description of FEMA 350 for the NC limit state, which was proposed for the steel frames may be regarded as convenient for the reinforced concrete bare frames. Whereas the collapse mechanism was already produced for the OGS frame at the NC limit of FEMA 350 (Fig. 10(b)). It may be concluded that the definition of NC limit state at an earlier stage may be regarded as more appropriate for the OGS frame.

### 4.3. Comparison of SPO Analyses and IDA Results

The base shear-roof drift relationships obtained by SPO and IDA (median) are presented together in Fig. 11 for each model. Similar to the statement of Vamvatsikos and Cornell [22], when the intensity measure and engineering demand parameters are selected as those in this study, the capacity diagrams achieved by both SPO and IDA methods are almost identical in the initial region. Yet, the base shear (or $S_a$ determined by Eqn. (5)) capacities determined by the SPO and IDA are also quite similar which is in contradiction to the results of Vamvatsikos and Cornell [22]. Eventually, the curves of each analysis method begin to differentiate after the ultimate base shear capacity is reached. This result was more significant in the case of OGS.

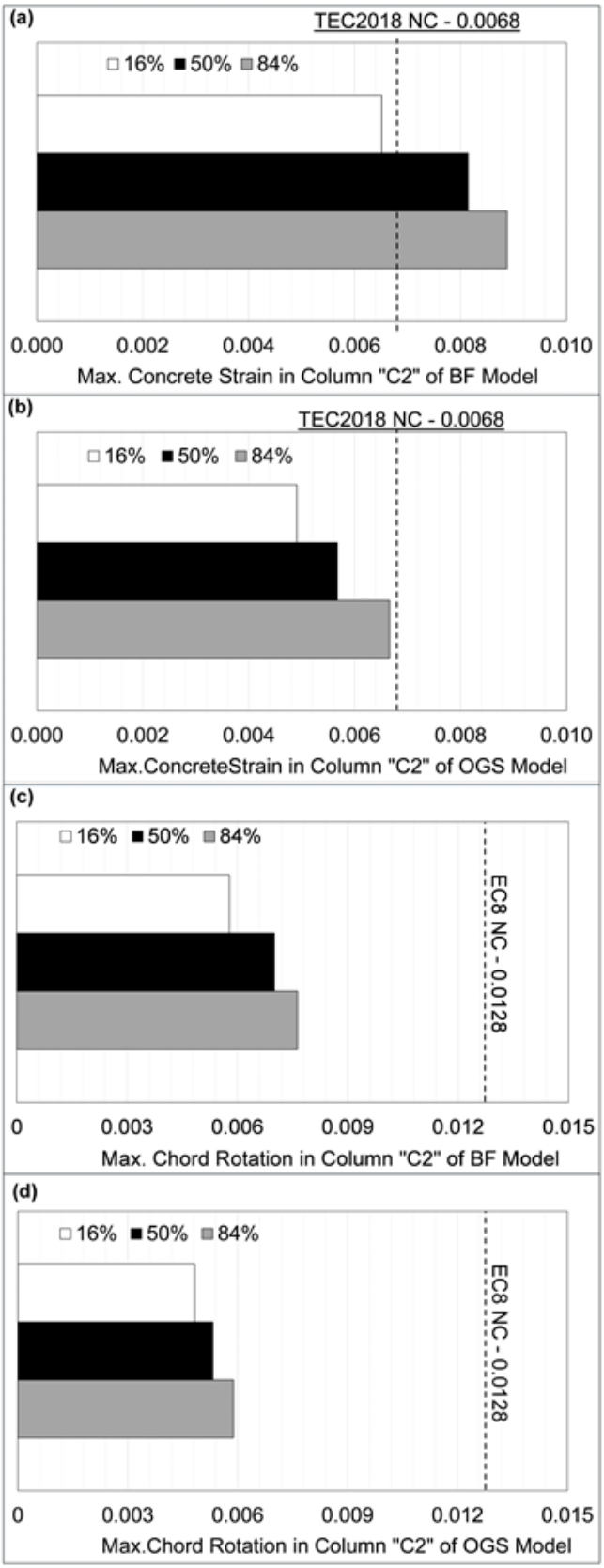


**Figure 8.** The comparison of NC limit state definitions of FEMA 350, TEC, and Eurocode 8

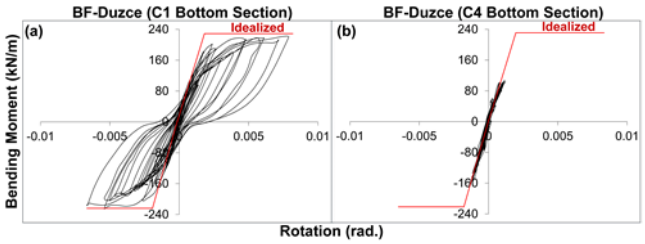


**Figure 9.** Moment-rotation behavior at the initial sections of columns (a) C1 and (b) C4 at the NC limit of FEMA 350

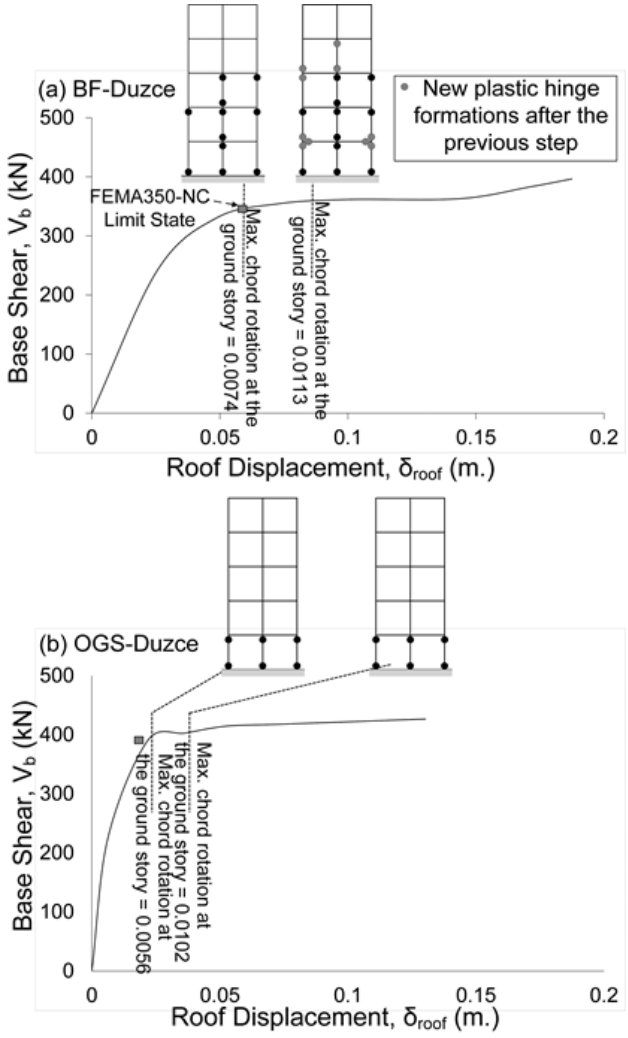


**Figure 10.** The plastic hinge formations of the (a) BF and (b) OGS models at two stages of IDA for Duzce record

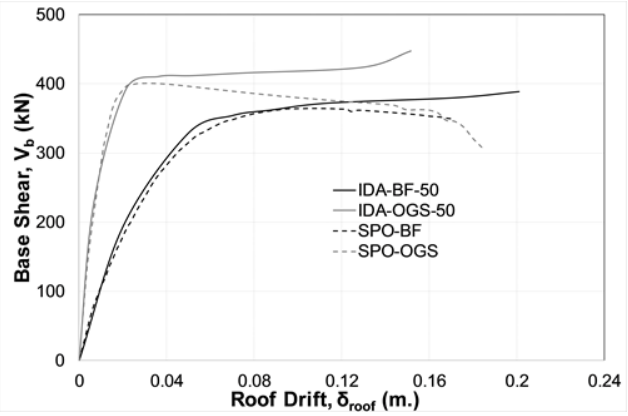


**Figure 11.** Base shear-roof drift diagrams of SPO and IDA (median)

In Fig. 12, the maximum concrete strain and chord rotation of column C2 are compared for three steps of the response (i.e., in the case of Imperial Valley record exemplarily). The local demand parameters of the BF derived from the SPO and IDA were very approximate at the initial part of the response and started to differentiate as the related capacity curves separate (Fig. 12). This was more considerable for the concrete strain, which may clarify the more conservative assessment conducted by the SPO according to the chord rotation (i.e., concrete strain remains lower in the SPO). Although the separation of SPO and IDA curves after the ultimate capacity is more distinct for the OGS, the inelastic demand values determined by the two methods at the same roof drift are quite approximate in all regions of the response of this model. This may be related to the concentration of demand at the story level without infills. The measure of the scattering of damage between the stories of BF may be dissimilar for the SPO and IDA which may result in the demands changing at different stages of response in this model.

## 5. Conclusion

A reinforced concrete bare and OGS frame were analyzed using SPO and IDA regarding the NC limit state descriptions of different seismic codes. The two different analyses methods were also compared in terms of this evaluation. It should be noted that the presented results were obtained according to the assumptions of the study.

The assessment by SPO provided much larger demands for the OGS frame as may be expected, although the corresponding target displacement was smaller for the OGS compared to BF. According to the SPO analyses, it may be stated that the seismic assessment with regard to the definition of Eurocode 8 in terms of chord rotation is more conservative than the definition of TEC [12] in terms of concrete strain. This statement is more considerable for the BF model.

The NC limit state described by FEMA 350 which is suggested actually for the steel frames and based on a graphical interpretation of the IDA results was also suitable for the RC bare frame considered in this study. However, the same conclusion may not be valid for the OGS frame due to the plastic hinge formations that indicate an early column-sidesway mechanism in this model. It may be more appropriate to define the near-collapse at an earlier stage on the IDA curve for the RC frames with OGS. As opposed to the conclusion from the SPO analyses, the concrete strain limit of TEC [12] is more conservative in describing the near-collapse for the columns of bare RC frames considering the IDA results, which is not the case for the frame with OGS. The chord rotation limit of Eurocode 8 seems to describe the near-collapse of the columns at a much later stage on the IDA curves considering both BF and OGS models. The quite early signs of collapse without producing considerable inelastic deformations should be regarded more conservatively during the seismic assessment of existing nonductile OGS buildings.

The differences in the assessment according to different codes by using either SPO or IDA results may be

understood after a closer look at the local demands of the ground story columns at different stages of the results. Although the global SPO capacity and IDA curves are very close for the bare RC frame, the dissociation of local demands obtained by these two analysis methods increases as the inelastic actions progress within the structure. This was more distinct for the concrete strain which was significantly smaller in the SPO results of BF in comparison to IDA. On the other hand, the global SPO and IDA curves of OGS differ from each other considerably during the inelastic response. Yet, the local demand values are close at all stages of the two analysis methods.

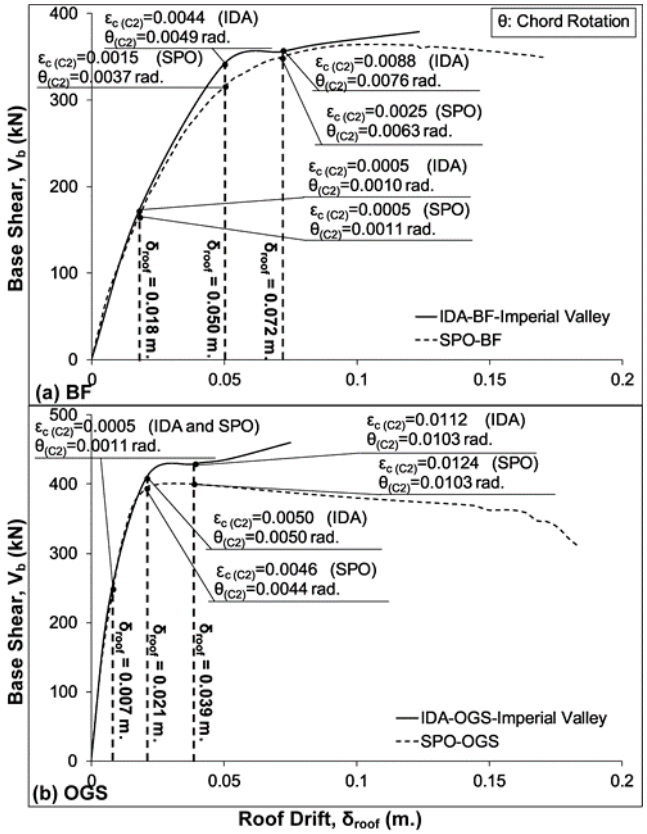


**Figure 12.** The maximum concrete strain and chord rotation of column C2 at various steps of the SPO and IDA curves: (a) for BF and (b) for OGS

**Acknowledgement**

This work was supported by the Adnan Menderes University Scientific Research Projects Commission [grant number MF-19013].

**Author contributions**

**Emre Akın:** Conceptualization, Methodology, Software, Writing-Original draft preparation, Validation. **Emad Kanas:** Data curation, Writing-Original draft preparation, Visualization, Investigation, Writing-Reviewing and Editing.

**Conflicts of interest**

The authors declare no conflicts of interest.

**References**

1. Asteris, P. G. (2003). Lateral Stiffness of Brick Masonry Infilled Plane Frames. Journal of Structural Engineering, American Society of Civil Engineers (ASCE), 129(8), 1071–1079. https://doi.org/10.1061/(ASCE)0733-9445(2003)129:8(1071)
2. Cavaleri, L. & Di Trapani, F. (2014). Cyclic response of masonry infilled RC frames: Experimental results and simplified modeling. Soil Dynamics and Earthquake Engineering, 65, 224–242. https://doi.org/10.1016/j.soildyn.2014.06.016
3. Comite Euro-International du Beton (CEB) (1996). RC Frames Under Earthquake Loading: State of the Art Report. Thomas Telford, London, UK.
4. Dolšek, M., & Fajfar, P. (2008). The effect of masonry infills on the seismic response of a four storey reinforced concrete frame-a probabilistic assessment. Engineering Structures, 30(11), 3186–3192. https://doi.org/10.1016/j.engstruct.2008.04.031
5. Hashemi, A., & Mosalam, K. M. (2006). Shake-table experiment on reinforced concrete structure containing masonry infill wall. Earthquake Engineering and Structural Dynamics, 35(14), 1827–1852. https://doi.org/10.1002/eqe.612
6. Mehrabi, A. B, Shing, P. B., Schuller, M. P., & Noland, J. L. (1996). Experimental Evaluation of Masonry-Infilled RC Frames. Journal of Structural Engineering, 122(3), 228–237. https://doi.org/10.1061/(ASCE)0733-9445(1996)122:3(228)
7. Negro, P. & Verzeletti, G. (1996). Effect of infills on the global behaviour of R/C frames: Energy considerations from pseudodynamic tests. Earthquake Engineering and Structural Dynamics, 25(8), 753–773. https://doi.org/10.1002/(SICI)1096-9845(199608)25:8<753::AID-EQE578>3.0.CO;2-Q
8. Dolšek, M., & Fajfar, P. (2001). Soft storey effects in uniformly infilled reinforced concrete frames. Journal of Earthquake Engineering, 5(1), 12. https://doi.org/10.1080/13632460109350383
9. Negro, P., & Colombo, A. (1997). Irregularities induced by nonstructural masonry panels in framed buildings. Engineering Structures, 19(7), 576–585. https://doi.org/10.1016/S0141-0296(96)00115-0
10. Akın, E. (2019). Open ground story in properly designed reinforced concrete frame buildings with shear walls. Structures, 20, 822-831. https://doi.org/10.1016/j.istruc.2019.07.003
11. Eurocode 8 (2005). European Standard EN 1998-3:2005: Design of structures for earthquake resistance - Part 3: Assessment and retrofitting of buildings. Comite Europeen de Normalisation, Brussels, Belgium.
12. TEC (2018). Turkish Earthquake Code for Buildings. Republic of Turkey Prime Ministry Disaster and Emergency Management Authority, Ankara, Turkey.

13. SeismoStruct (2020). A computer program for static and dynamic nonlinear analysis of framed structures. Seismosoft Ltd. https://seismosoft.com
14. Kadaş, K. (2006). Influence of idealized pushover curves on seismic response. MSc Thesis, Middle East Technical University, Graduate School of Natural and Applied Sciences, Ankara, Turkey, 320p.
15. Mander, J. B., Priestley, M. J. N., & Park, R. (1988). Theoretical Stress-Strain Model for Confined Concrete. Journal of Structural Engineering, 114(8), 1804–1826. https://doi.org/10.1061/(ASCE)0733-9445(1988)114:8(1804)
16. Martínez-Rueda, J. E., & Elnashai, A. S. (1997). Confined concrete model under cyclic load. Materials and Structures, 30(3), 139–147. https://doi.org/10.1007/BF02486385
17. ACI (American Concrete Institute) (2008). Building code requirements for structural concrete (ACI 318M-08) and Commentary. Farmington Hills, MI, USA.
18. American Society of Civil Engineers (ASCE) (2000). Prestandard and commentary for the seismic rehabilitation of buildings (FEMA 356). Washington, D.C., USA
19. TEC (2007). Turkish Earthquake Code for Buildings. Republic of Turkey Prime Ministry Disaster and Emergency Management Authority, Ankara, Turkey.
20. SeismoMatch (2018). A computer program for spectrum matching of earthquake records. Seismosoft Ltd. https://seismosoft.com
21. FEMA-350 (2000). Recommended Seismic Design Criteria for New Steel Moment-Frame Buildings. Washington, D.C., USA.
22. Vamvatsikos, D., & Cornell, C. A. (2005). Direct estimation of the seismic demand and capacity of multidegree-of-freedom systems through incremental dynamic analysis of single degree of freedom approximation. Journal of Structural Engineering, 131(4). https://doi.org/10.1061/(ASCE)0733-9445(2005)131:4(589)